Check for updates

Efficient catalytic direct C–H hydroxylation of benzene by graphite-supported μ-nitrido-bridged iron phthalocyanine dimer†

Yasuyuki Yamada, [iD] *[ab] Yoshiki Uno,[a] Chee-Ming Teoh, [iD][a] Hirotaka Ohkita,[b] Yuka Toyoda,[b] Akiko Sakata,[b] Yutaka Hitomi [iD][c] and Kentaro Tanaka [iD] *[ad]

Hydroxylation of benzene directly into phenol without converting it into other compounds by using a metal complex-based oxidation catalyst is challenging because of the chemical stability of benzene. We demonstrated that a graphite-supported μ-nitrido-bridged iron phthalocyanine dimer, which acts as a potent iron–oxo-based molecular methane oxidation catalyst, can efficiently catalyze the direct benzene hydroxylation at 25 °C in an aqueous acetonitrile solution containing excess H₂O₂. It was confirmed that the catalytic benzene hydroxidation activity of the graphite-supported μ-nitrido-bridged iron phthalocyanine dimer was significantly higher than that of the silica gel-supported μ-nitrido-bridged iron phthalocyanine dimers.

1. Introduction

High-valent iron–oxo species are an important class of reactive intermediates that are often involved in the oxidation of organic substrates by natural oxygenases such as methane monooxygenase and cytochrome P450.[1–3] Inspired by the fact that these oxygenases achieve difficult C–H activation of organic molecules by utilizing high-valent iron–oxo species under mild reaction conditions, a large variety of artificial iron–oxo-based molecular catalysts have been created.[3–6] Artificial iron–oxo-based molecular catalysts are expected to be applicable to the catalytic oxidation reactions of various organic compounds.

[a] Department of Chemistry, Graduate School of Science, Nagoya University, Furo-cho, Chikusa-ku, Nagoya 464-8602, Japan.
E-mail: yamada.yasuyuki.i6@f.mail.nagoya-u.ac.jp, kentaro@chem.nagoya-u.ac.jp
[b] Research Center for Materials Science, Nagoya University, Furo-cho, Chikusa-ku, Nagoya 464-8602, Japan
[c] Department of Molecular Chemistry and Biochemistry, Graduate School of Science and Engineering, Doshisha University, Kyotanabe, Kyoto, 610-0321, Japan
[d] Research Institute for Quantum and Chemical Innovation, Institutes of Innovation for Future Society, Nagoya University, Furo-cho, Chikusa-ku, Nagoya 464-8602, Japan
† Electronic supplementary information (ESI) available: Detailed experimental data of oxidation experiments. See DOI: https://doi.org/10.1039/d4cy00661e

μ-Nitrido-bridged iron porphyrinoid dimers such as μ-nitrido-bridged iron phthalocyanine dimers are an important class of potent artificial iron–oxo-based molecular catalysts.[7–23] For instance, the iron–oxo species of a μ-nitrido-bridged iron phthalocyanine dimer **1═O**, which can be generated by treating **1** or its 1e⁻-oxidized product **1⁺** with H₂O₂ in an acidic aqueous solution, have such a high oxidizing ability that can even catalytically activate the inert C–H bonds of methane at temperatures lower than 100 °C (Fig. 1a).[7–9,11,13,14,18] Moreover, we recently demonstrated that the catalytic activity of **1** is significantly enhanced by stacking on the π-surface of graphite.[22] We considered that stacking interaction between **1** and graphite would change the electronic structure of both of **1** and **1═O** to affect the
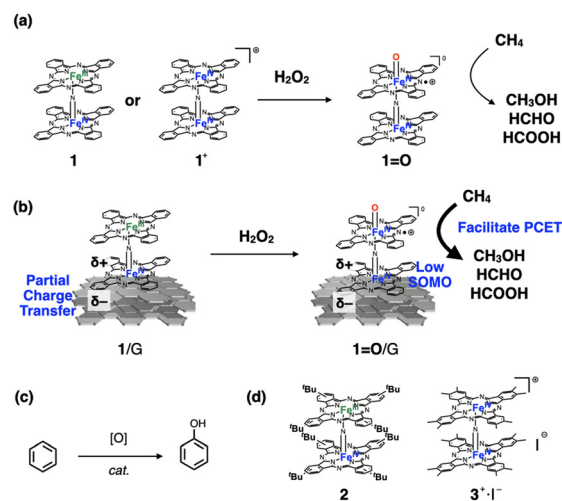

Fig. 1 (a) Formation of a high-valent iron–oxo species **1═O** from **1** or **1⁺** for C–H activation of methane. (b) Efficient C–H activation of methane by a graphite-supported high-valent iron–oxo species **1═O/G** generated from a μ-nitrido-bridged iron phthalocyanine dimer stacked on graphite **1/G**. (c) Direct benzene hydroxylation reaction. (d) μ-Nitrido-bridged iron phthalocyanine dimers **2** and **3⁺·I⁻** that catalyze benzene hydroxylation.

4854 | *Catal. Sci. Technol.*, 2024, **14**, 4854–4859

This journal is © The Royal Society of Chemistry 2024

catalytic activity of **1**. In order to confirm this assumption, we compared the catalytic methane oxidation activity of the graphite-supported μ-nitrido-bridged iron phthalocyanine dimer **1** (**1**/G) with that of **1** or **1**⁺·I⁻ on silica gel-support (**1**/SiO₂ or **1**⁺·I⁻/SiO₂). Actually, **1**/G showed more than 70 times higher methane oxidation activity than **1**/SiO₂ or **1**⁺·I⁻/SiO₂ in an acidic aqueous solution at 60 °C. A detailed examination of **1**/G *via* electrochemistry and DFT calculations suggested that the high catalytic activity of **1**/G is derived from the electronic interaction between the catalyst molecule and graphite, to cause the partial charge transfer from the catalyst molecule to graphite without changing the redox states of the iron ions in the μ-nitrido-bridged iron phthalocyanine dimer and also lower the singly occupied molecular orbital (SOMO) level of the catalyst molecule on graphite. As a result, electron transfer from methane to **1**=O/G in the proton-coupled electron transfer process could have been facilitated (Fig. 1b).

In this manuscript, we report the direct C–H bond activation of benzene by **1**/G. As benzene is a chemically stable compound having a high C–H bond dissociation energy of 113 kcal mol⁻¹, direct C–H bond activation of benzene at lower temperature is considered as a difficult C–H activation.[24–30] A. B. Sorokin *et al.* confirmed that **2** can catalytically oxidize benzene to afford a mixture of phenol and *p*-quinone in a homogeneous aqueous CH₃CN solution containing H₂O₂ at 60 °C.[10] Our group also demonstrated that a monocationic μ-nitrido-bridged iron–phthalocyanine dimer having 16 electron-donating peripheral methyl groups on SiO₂ (**3**⁺·I⁻/SiO₂) showed 10 times higher catalytic benzene oxidation activity than at 40 °C in an aqueous CH₃CN solution containing H₂O₂.[20] Considering that **1**/G showed considerably higher catalytic methane oxidation activity than those of **1** or **1**⁺, we became interested in comparing the catalytic benzene oxidation activity of **1**/G with that of **3**⁺·I⁻/SiO₂. Herein, we compared the catalytic activity of **1**/G with that of **3**⁺·I⁻/SiO₂ under the same reaction conditions and demonstrated that **1**/G is effective for the efficient catalytic oxidation of benzene at 25 °C.

2. Results and discussion

The graphite-supported catalyst **1**/G was prepared according to our previous report; that is, a monocationic form of μ-nitrido-bridged iron phthalocyanine dimer (**1**⁺·I⁻) was heated with graphite in pyridine at 80 °C to adsorb the catalyst molecule on graphite, followed by washing with aqueous trifluoroacetic acid to remove pyridine.[22,31] In our previous report, we confirmed that the adsorbed μ-nitrido-bridged iron phthalocyanine dimer was reduced by one electron by graphite to become its neutral form (**1**) using X-ray photoelectron spectroscopy (XPS) spectroscopy and electrochemical analysis.[22]

Benzene oxidation reactions were performed in a CH₃CN solution containing excess amounts of benzene (450 mM), TFA (141 mM), and H₂O₂ (1.04 M) at 25 °C in the presence of

1⁺·I⁻/SiO₂, **3**⁺·I⁻/SiO₂ or **1**/G (49 μM as **1**⁺, **3**⁺, or **1**). A sufficient amount of TFA was added because acidic conditions are effective in producing high-valent iron–oxo species efficiently.[7–23] The reaction was monitored and the oxidized compounds were detected by ¹H-NMR spectroscopy.

After a 2 h oxidation by **1**/G at 25 °C, the production of phenol was observed, as shown in Fig. 2a. A low concentration of *p*-quinone, which can be generated by the oxidation of 1,4-dihydroxybenznene, was also observed, whereas other types of overoxidized products, such as *o*-quinone and 1,2-, 1,3-, or 1,4-dihydroxybenzenes, which can be produced by hydroxylation of phenol, were not found. It is considered that the peak observed at 8.14 ppm, which is assignable to HCOOH, was derived from CH₃CN because it was observed in the absence of benzene, as shown in Fig. S1,† suggesting that **1**/G has such a high oxidizing ability that it can oxidize chemically inert CH₃CN even at room temperature. We also performed benzene oxidation using H₂O as the solvent instead of CH₃CN at 25 °C for 4 h (a two-phase reaction; for details, see ESI† page S4) to confirm that a significant amount of phenol was produced, but *p*-quinone was not observed under these reaction conditions (entry 14 in Table 1 and Fig. S2†). In an aqueous solution, the graphite surface can be surrounded by benzene molecules because of the hydrophobicity of both the graphite surface and benzene. We assumed that this might have caused the lower production rate of *p*-quinone by maintaining a high effective concentration of benzene around the graphite surface.

The time dependence of the concentrations of phenol and *p*-quinone produced in the reaction at 25 °C in CH₃CN was summarized in Fig. 2b and Table 1. Because benzene oxidation can proceed in a stepwise manner from phenol to *p*-quinone, we calculated the turnover number for benzene consumption (TON$_{BC}$), according to the following eqn (i), where C_{phenol} and $C_{p\text{-quinone}}$, and C_{Cat} represent the concentrations of phenol, *p*-quinone, and the catalyst molecule, respectively.

$$\text{TON}_{BC} = (C_{phenol} + C_{p\text{-quinone}})/C_{Cat} \quad \text{(i)}$$

As shown in Fig. 2c, the amount of TON$_{BC}$ increased almost linearly during the initial stage of the reaction (up to 2 h) and then gradually saturated. The initial linear increase in TON$_{BC}$ suggests that **1**/G worked stably under these reaction conditions, as in the case of CH₄ oxidation in an acidic aqueous solution containing excess H₂O₂.[22] We also confirmed that **1**/G was reusable after the reaction at 25 °C for 1 h with its catalytic activity almost unchanged from that before use (95%) as summarized in page S6 in the ESI.† The gradual saturation of TON$_{BC}$ was presumably due to the over-oxidation of *p*-quinone and a decrease in the concentration of H₂O₂. In our previous study, we confirmed that the concentration of H₂O₂ gradually decreases through the catalase reaction by **1**/G in an acidic aqueous solution containing excess H₂O₂.[22] Oxidation of CH₃CN could also contribute to the decrease in the H₂O₂ concentration. At an
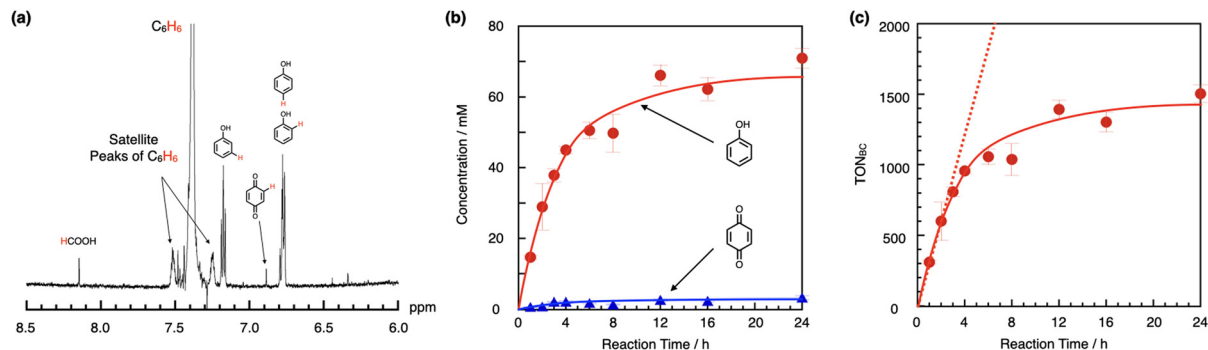
Fig. 2 (a) ^{1}H-NMR spectrum of a reaction mixture of benzene oxidation by **1**/G at 25 °C for 2 h. (b) Time dependence of the concentrations of phenol (filled red circle) and *p*-quinone (filled blue triangle) observed in the benzene oxidation reaction performed at 25 °C. (c) Time dependence of TON_{BC} (definition is shown in the main text) for the benzene oxidation reaction at 25 °C. Initial reaction condition: [benzene] = 450 mM, [TFA] = 141 mM, [H_2O_2] = 1.04 M in CH_3CN (1.0 mL) containing 10 mg of **1**/G ([**1**] = 49 μM). Error bars indicate standard deviations of the three independent reactions.

Table 1 Results of benzene oxidation reactions performed at 25 °C. Initial reaction condition: [benzene] = 450 mM, [TFA] = 141 mM, [H_2O_2] = 1.04 mM, CH_3CN (1.0 mL), 10 mg of **1**/G, **1**$^+$·I$^-$/SiO_2, **3**$^+$·I$^-$/SiO_2, or **1**/SiO_2. ([**1**] = [**1**$^+$·I$^-$] = [**3**$^+$·I$^-$] = 49 μM). The numbers in the parenthesis indicate the standard deviations of the three independent reactions. The reaction in the presence of 102 mM DMPO (entry 10) was performed only once

Entry	Catalyst	Reaction time/h	Solvent	Additive	[Phenol]/mM	[*p*-Quinone]/mM	TON_{BC}
1	**1**/G	1	CH_3CN	⋯	14.7 (0.53)	0.6 (0.1)	310 (13)
2	**1**/G	2	CH_3CN	⋯	28.9 (6.6)	0.8 (0.2)	601 (137)
3	**1**/G	3	CH_3CN	⋯	37.8 (1.8)	2.1 (0.1)	851 (34)
4	**1**/G	4	CH_3CN	⋯	45.0 (1.0)	2.1 (0.4)	955 (18)
5	**1**/G	6	CH_3CN	⋯	50.6 (2.4)	1.8 (0.2)	1057 (54)
6	**1**/G	8	CH_3CN	⋯	49.8 (5.4)	1.4 (0.1)	1037 (114)
7	**1**/G	12	CH_3CN	⋯	66.1 (2.9)	2.6 (0.3)	1393 (66)
8	**1**/G	16	CH_3CN	⋯	62.2 (3.3)	2.3 (0.2)	1303 (70)
9	**1**/G	24	CH_3CN	⋯	71.0 (2.8)	3.3 (0.5)	1504 (63)
10	**1**/G	2	CH_3CN	102 mM DMPO	18.7	n.d.	378
11	**3**$^+$·I$^-$/SiO_2	2	CH_3CN	⋯	3.43 (0.88)	n.d.	69 (18)
12	**1**$^+$·I$^-$/SiO_2	2	CH_3CN	⋯	n.d.	n.d.	0 (0)
13	**1**/SiO_2	2	CH_3CN	⋯	n.d.	n.d.	0 (0)
14	**1**/G	4	H_2O/benzene	⋯	11.3 (2.4)	n.d.	239 (51)

elevated temperature (80 °C), the concentrations of over-oxidized products, including *p*-quinone, maleic acid, oxaloacetic acid, and formic acid, increased, as shown in Fig. S3.† These results indicate that **1**/G has such a high oxidizing ability that it can even decompose the benzene ring in the presence of H_2O_2, as observed with **3**$^+$·I$^-$/SiO_2.

The catalytic benzene oxidation rate of **1**/G was compared with those of **1**$^+$·I$^-$/SiO_2 and **3**$^+$·I$^-$/SiO_2 at 25 °C for 2 h of oxidation (entries 2, 11, and 12 in Table 1). **1**$^+$·I$^-$/SiO_2 did not show apparent benzene oxidation activity under these reaction conditions (entry 12 in Table 1). While it was observed that **3**$^+$·I$^-$/SiO_2 catalyzed benzene oxidation even at room temperature (entry 11 in Table 1), **1**/G showed a considerably higher benzene oxidation activity (entry 2 in Table 1). We previously reported that the catalytic CH_4 oxidation activity of **1**/SiO_2 was nearly identical to that of **1**$^+$·I$^-$/SiO_2 in an aqueous solution containing excess H_2O_2 and TFA at 60 °C.[22] Moreover, in this research, we confirmed that both of **1**$^+$·I$^-$/SiO_2 and **1**/SiO_2 did not show benzene oxidation activity at 25 °C in aqueous CH_3CN solutions containing excess H_2O_2 and TFA (see entries 12 and 13 in Table 1).

Considering that small amounts of HCOOH, which were generated from CH_3CN, were observed for both of the reactions of entry 12 and 13, the reaction without using CH_3-CN and/or a longer reaction time should be necessary for **1**$^+$·I$^-$/SiO_2 and **1**/SiO_2 to show apparent benzene oxidation activities at room temperature. Although it was difficult to check the benzene oxidation activity of **3**/SiO_2, where a neutral complex **3** is used as the catalyst molecule, because **3** is easily oxidized in the air, it seems that the high catalytic activity of **1**/G is not derived from the difference in the oxidation state of the μ-nitrido-bridged iron phthalocyanine dimer but from the significant effect of the graphite substrate on the electronic structure of the μ-nitrido-bridged iron phthalocyanine dimer.

To further understand the reaction mechanism of benzene oxidation by **1**/G, the initial oxidation rates of several benzene derivatives were examined and compared with those of benzene, as shown in Fig. 3 and Table 2. A linear correlation with a negative slope was observed in the Hammett plot.[32] This result apparently indicates the electrophilic nature of the reactive intermediate in the oxidation reaction of the
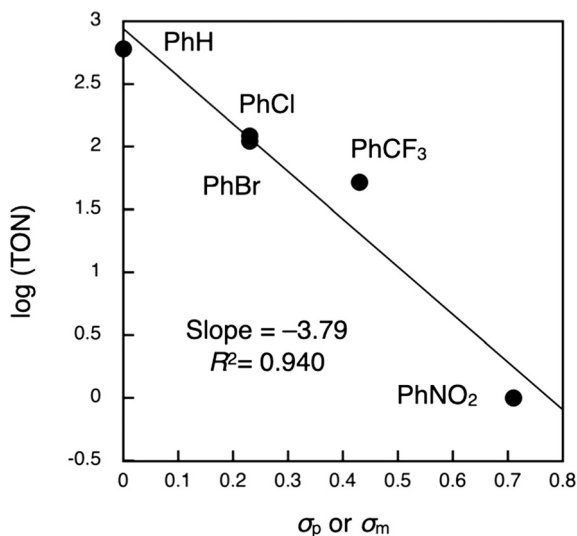
4856 | *Catal. Sci. Technol.*, 2024, **14**, 4854–4859

This journal is © The Royal Society of Chemistry 2024

Fig. 3 Hammett plot of the turnover numbers (TONs) for the oxidation of benzene derivatives by **1**/G. In the Hammett plot, the following substrates were used: PhH (σ_p = 0.00), PhCl (σ_p = 0.23), PhBr (σ_p = 0.23), PhCF$_3$ (σ_m = 0.43), PhNO$_2$ (σ_m = 0.71). (Ref. 32) for benzene (PhH) oxidation, TON$_{BC}$ at 2 h oxidation (entry 2 in Table 1) was used as the TON.

benzene derivatives. In our previous paper, we determined the Hammett ρ value of **3**$^+$·I$^-$/SiO$_2$ in a similar acidic aqueous CH$_3$CN solution at 40 °C to be −1.14, which is less negative than that for **1**/G at 25 °C (−3.79).[20] These results could suggest that the high-valent iron oxo species of **1**/G (**1**=O/G) become more electrophilic in the benzene oxidation than that of **3**$^+$·I$^-$/SiO$_2$ because of the interaction between **1** and graphite(G).[33]

We also examined the kinetic isotope effects (KIE) by comparing the initial oxidation rates (1 h oxidation) of C$_6$H$_6$ and C$_6$D$_6$. The obtained KIE value (k_H/k_D) was 1.0 (for details, see ESI† page S12), implying that the C–H bond cleavage is not involved in the turnover-limiting step. It is known that Fenton-type reaction, where a hydroxyl radical (·OH) is the reactive intermediate, shows KIE values of 1.7–1.8,[34] which are apparently higher than that of the benzene oxidation by **1**/G (1.0). Additionally, it was confirmed that the benzene oxidation by **1**/G was not significantly quenched by the

addition of an excess amount of 5,5-dimethyl-1-pyrroline-N-oxide (DMPO), a well-known radical scavenger (entry 10 in Table 1).[27,29] These results also imply that the high-valent iron–oxo species **1**=O/G generated from **1**/G should be the reactive intermediate, as observed in the case of methane oxidation.[22]

In the case of CH$_4$ oxidation, oxidation by high-valent iron–oxo species generally proceeds through a proton-coupled electron transfer (PCET) mechanism, wherein proton and electron abstractions from the substrate occur in a concerted manner.[35,36] The results of benzene oxidation suggest that the abstraction of the π-electron of the benzene ring by **1**=O/G could be involved in the turnover-limiting step of benzene oxidation, whereas the opposite should be observed for the proton abstraction process. Possible reaction mechanisms are summarized in Fig. 4. First, the high-valent terminal iron–oxo species **1**=O/G is produced through the reaction of **1**/G with H$_2$O$_2$. **1**=O/G act as the reactive intermediate to cause the successive C–O bond formation coupled with electron transfer between **1**=O/G and benzene. Our previous DFT calculation on **1**/G suggested that interaction of **1** with graphite support cause SOMO stabilization and partial charge transfer from **1** to graphite. Since it is reported that **1**=O also has a SOMO distributed mainly over O=Fe–N=Fe center,[7,37] stabilization of SOMO of **1**=O with partial charge transfer could also occur on graphite support as described in Fig. 4.[22] This electronic state can enhance the electron abstraction ability of the high-valent iron–oxo species compared to those of **1**$^+$·I$^-$/SiO$_2$ and **3**$^+$·I$^-$/SiO$_2$ to facilitate the successive C–O bond formation coupled with electron transfer between **1**=O/G and benzene.[38] This assumption does not contradict the fact that the Hammett ρ value of **1**/G (−3.79) was much more negative than that observed for **3**$^+$·I$^-$/SiO$_2$ (−1.14).

Conclusions

In conclusion, we investigated the oxidation reaction of benzene in an aqueous CH$_3$CN solution containing excess H$_2$O$_2$ and TFA by using a graphite-supported μ-nitrido-bridged iron phthalocyanine dimer (**1**/G) as a catalyst. It was demonstrated that **1**/G efficiently oxidized benzene into

Table 2 Summary of the oxidation reactions of benzene derivatives by **1**/G at 25 °C for 2 h. Turnover numbers of benzene derivatives (TONs) were calculated from the total concentration of the oxidized products obtained from the results of ^{1}H-NMR measurements. N.d. indicates "not detected" in the ^{1}H-NMR measurement. Details of the oxidation reaction is summarized in page S7 in the ESI†

Entry	Benzene derivative	P1/mM	P2/mM	P3/mM	Q1/mM	TON (total)
1	PhCl (**X** = Cl)	2.67 (0.29)	0.88 (0.25)	2.33 (0.11)	n.d.	122 (13)
2	PhBr (**X** = Br)	2.11 (0.45)	1.30 (0.25)	1.93 (0.10)	n.d.	111 (15)
3	PhCF$_3$ (**X** = CF$_3$)	0.20 (0.28)	1.61 (0.07)	0.72 (0.14)	n.d.	52 (3)
4	PhNO$_2$ (**X** = NO$_2$)	0.04 (0.06)	0.01 (0.01)	0.00 (0.00)	n.d.	1 (1)

This journal is © The Royal Society of Chemistry 2024

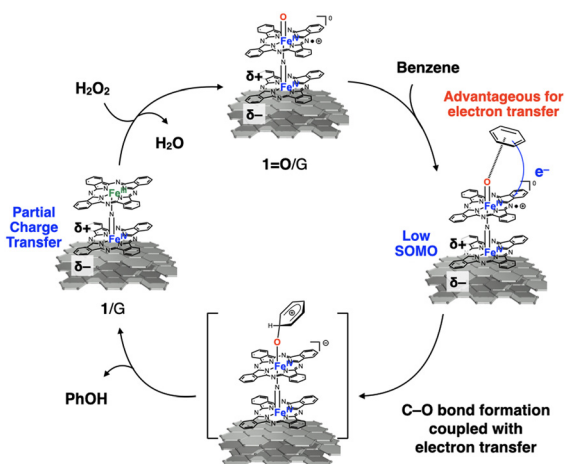*Catal. Sci. Technol.*, 2024, **14**, 4854–4859 | **4857**

Fig. 4 Possible reaction mechanism of the benzene oxidation by **1**/G.

phenol and *p*-benzoquinone even at 25 °C and its catalytic activity was much higher than that of silica gel-supported catalysts $\mathbf{1}^{+}\cdot\mathrm{I}^{-}/\mathrm{SiO}_2$ and $\mathbf{3}^{+}\cdot\mathrm{I}^{-}/\mathrm{SiO}_2$ in the same reaction conditions. These results apparently indicate the significant effect of the graphite support on the catalytic oxidation activity of µ-nitrido-bridged iron phthalocyanine dimer, which can facilitate the electron transfer from benzene to **1**/G.

Data availability

The authors confirm that the data supporting the findings of this study are available within the article and its ESI.†

Conflicts of interest

There are no conflicts to declare.

Acknowledgements

References

1 C. E. Tinberg and S. J. Lippard, *Acc. Chem. Res.*, 2011, **44**, 280–288.

2 S. Shaik, H. Hirao and D. Kumar, *Acc. Chem. Res.*, 2007, **40**, 532–542.

3 V. C.-C. Wang, S. Maji, P. P.-Y. Chen, H. K. Lee, S. S.-F. Yu and S. I. Chan, *Chem. Rev.*, 2017, **117**, 8574–8621.

4 A. R. McDonald and L. Que Jr., *Coord. Chem. Rev.*, 2013, **257**, 414–428.

5 V. A. Larson, B. Battistella, K. Ray, N. Lehnert and W. Nam, *Nat. Rev. Chem.*, 2020, **4**, 404–419.

6 R. A. Baglia, J. P. T. Zaragoza and D. P. Goldberg, *Chem. Rev.*, 2017, **117**, 13320–13352.

7 P. Afanasiev and A. B. Sorokin, *Acc. Chem. Res.*, 2016, **49**, 583–593.

8 A. B. Sorokin, *Catal. Today*, 2021, **373**, 38–58.

9 A. B. Sorokin, E. V. Kudrik and D. Bouchu, *Chem. Commun.*, 2008, 2562–2564.

10 E. V. Kudrik and A. B. Sorokin, *Chem. – Eur. J.*, 2008, **14**, 7123–7126.

11 E. V. Kudrik, P. Afanasiev, L. X. Alvarez, P. Dubourdeaux, M. Clémancey, J.-M. Latour, G. Blondin, D. Bouchu, F. Albrieux, S. E. Nefedov and A. B. Sorokin, *Nat. Chem.*, 2012, **4**, 1024–1029.

12 L. X. Alvarez and A. B. Sorokin, *J. Organomet. Chem.*, 2015, **793**, 139–144.

13 Ü. İsci, A. S. Faponle, P. Afanasiev, F. Albrieux, V. Briois, V. Ahsen, F. Dumoulin, A. B. Sorokin and S. P. de Visser, *Chem. Sci.*, 2015, **6**, 5063–5075.

14 M. G. Quesne, D. Senthilnathan, D. Singh, D. Kumar, P. Maldivi, A. B. Sorokin and S. P. de Visser, *ACS Catal.*, 2016, **6**, 2230–2243.

15 N. Mihara, Y. Yamada, H. Takaya, Y. Kitagawa, K. Igawa, K. Tomooka, H. Fujii and K. Tanaka, *Chem. – Eur. J.*, 2019, **25**, 3369–3375.

16 Y. Yamada, K. Morita, N. Mihara, K. Igawa, K. Tomooka and K. Tanaka, *New J. Chem.*, 2019, **43**, 11477–11482.

17 Y. Yamada, J. Kura, Y. Toyoda and K. Tanaka, *New J. Chem.*, 2020, **44**, 19179–19183.

18 Y. Yamada, J. Kura, Y. Toyoda and K. Tanaka, *Dalton Trans.*, 2021, **50**, 6718–6724.

19 Y. Yamada, Y. Miwa, Y. Toyoda, T. Yamaguchi, S. Akine and K. Tanaka, *Dalton Trans.*, 2021, **50**, 16775–16781.

20 Y. Yamada, C.-M. Teoh, Y. Toyoda and K. Tanaka, *New J. Chem.*, 2022, **46**, 955–958.

21 Y. Yamada, Y. Miwa, Y. Toyoda, Q. M. Phung, K. Oyama and K. Tanaka, *Catal. Sci. Technol.*, 2023, **13**, 1725–1734.

22 Y. Yamada, K. Morita, T. Sugiura, Y. Toyoda, N. Mihara, M. Nagasaka, H. Takaya, K. Tanaka, T. Koitaya, N. Nakatani, H. Ariga-Miwa, S. Takakusagi, Y. Hitomi, T. Kudo, Y. Tsuji, K. Yoshizawa and K. Tanaka, *JACS Au*, 2023, **3**, 823–833.

23 Y. Yamada, Y. Miwa, Y. Toyoda, Y. Uno, Q. M. Phung and K. Tanaka, *Dalton Trans.*, 2024, **53**, 6556–6567.

24 R. V. Ottenbacher, E. P. Talsi and K. P. Bryliakov, *Appl. Organomet. Chem.*, 2020, **34**, e5900.

25 S. Fukuzumi and K. Ohkubo, *Asian J. Org. Chem.*, 2015, **4**, 836–845.

26 K. Yoshizawa, Y. Shiota and T. Yamabe, *J. Am. Chem. Soc.*, 1999, **121**, 147–153.

27 M. Yamada, K. D. Karlin and S. Fukuzumi, *Chem. Sci.*, 2016, **7**, 2856–2863.

4858 | *Catal. Sci. Technol.*, 2024, **14**, 4854–4859

This journal is © The Royal Society of Chemistry 2024

28 Y. Morimoto, S. Bunno, N. Fujieda, H. Sugimoto and S. Itoh, *J. Am. Chem. Soc.*, 2015, **137**, 5867–5870.

29 T. Tsuji, A. A. Zaoputra, Y. Hitomi, K. Mieda, T. Ogura, Y. Shiota, K. Yoshizawa, H. Sato and M. Kodera, *Angew. Chem., Int. Ed.*, 2017, **56**, 7779–7782.

30 Y. Shimoyama, T. Ishizuka, H. Kotani and T. Kojima, *ACS Catal.*, 2019, **9**, 671–678.

31 Y. Yamada, T. Sugiura, K. Morita, H. Ariga-Miwa and K. Tanaka, *Inorg. Chim. Acta*, 2019, **489**, 160–163.

32 C. Hansch, A. Leo and R. W. Taft, *Chem. Rev.*, 1991, **91**, 165–195.

33 S. P. de Visser, K. Oh, A.-R. Han and W. Nam, *Inorg. Chem.*, 2007, **46**, 4632–4641.

34 R. Augusti, A. O. Dias, L. L. Rocha and R. M. Lago, *J. Phys. Chem. A*, 1998, **102**, 10723–10727.

35 D. R. Weinberg, C. J. Gagliardi, J. F. Hull, C. F. Murphy, C. A. Kent, B. C. Westlake, A. Paul, D. H. Ess, D. G. McCafferty and T. J. Meyer, *Chem. Rev.*, 2012, **112**, 4016–4019.

36 J. E. M. N. Klein and G. Knizia, *Angew. Chem., Int. Ed.*, 2018, **57**, 11913–11917.

37 C. Comonban, E. V. Kudrik, V. Briois, J. C. Shwarbrick, A. B. Sorokin and P. Afanasiev, *Inorg. Chem.*, 2014, **53**, 11517–11530.

38 M. Asaka and H. Fujii, *J. Am. Chem. Soc.*, 2016, **138**, 8048–8051.

This journal is © The Royal Society of Chemistry 2024

Catal. Sci. Technol., 2024, **14**, 4854–4859 | **4859**